THE JOURNAL OF PHYSICAL CHEMISTRY Letters

pubs.acs.org/JPCL Letter

Nano Heat Pump Based on Reverse Thermo-osmosis Effect

Ji Li, Rui Long, Bo Zhang, Ronggui Yang, Wei Liu, and Zhichun Liu*

Cite This: J. Phys. Chem. Lett. 2020, 11, 9856−9861 Read Online

ACCESS | Metrics & More | Article Recommendations | Supporting Information

ABSTRACT: Heat pumps are widely used in domestic applications, agriculture, and industry. Here, we report a novel heat pump based on the reverse thermo-osmosis (RTO) effect in a nanoporous graphene (NPG) membrane. Through classical molecular dynamics (MD) simulation, we prove that the heat pump can transport mass and heat efficiently. The heat and mass fluxes are increased linearly with the hydraulic pressure provided. Ultrahigh heat fluxes of 6.2 ± 1.0 kW/cm^2 and coefficient of performance (COP) of 20.2 are obtained with a temperature increment of 5 K and a working pressure of 80 MPa. It is interesting that water molecules on the NPG membrane can evaporate in a cluster state, and the cluster evaporations reduce the vaporization enthalpy of the processes.

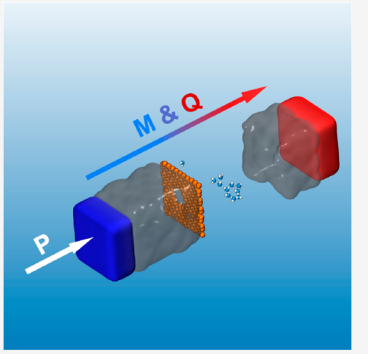

Thermal phenomena are ubiquitous, and thermal technology has improved the qualities of our life and production significantly. Around half of global energy is consumed for providing heat, and a tenth of electricity is used by air-conditioners and electric fans for cooling.[1] Heat pumps, including air-conditioners, refrigerators, air-source water heaters, and others, can supply heating or cooling energy by transfering heat between heat sources, which are much more efficient and environmentally friendly than getting heat directly from fossil fuels or electricity.[2] Vapor-compression heat pumps are the major types applied widely, and they consume power to drive vapor to condense and release heat to high-temperature sources. The performance of a heat pump can be valued by coefficient of performance (COP), the ratio of the heat movement to the energy consumed. A typical vapor-compression heat pump has a COP of approximately 3−4, greater than other types based on absorption or thermoelectric effect.[3,4] However, vapor-compression heat pumps face challenges, including noise level and flexibility.[5] Because traditional heating equipment still makes up most market share, it is important to improve the performance and usability of heat pumps to accelerate the substitution process and reduce our reliance on fossil fuel.[6]

While vapor-compression heat pumps are the devices that transfer heat and mass by driven force of power, as shown in Figure 1a, thermo-osmosis is the phenomenon that transfers mass driven due to the temperature difference between heat sources, coupling with heat transfer.[7,8] For a thermo-osmosis process in a vapor-gap membrane system, it consists of three physical processes: (1) liquid evaporation in the high-temperature side; (2) vapor transport across the membrane through the porous channel; and (3) vapor condensation in the low-temperature side.[9] Thermo-osmosis can generate a large hydraulic pressure difference across a membrane, and it is a promising method to convert thermal energy effectively by utilizing the pressure difference, called thermo-osmotic energy conversion (TOEC).[10−12] The ideal power generation efficiency of TOEC can be close to Carnot efficiency if reducing heat loss and temperature polarization, which can be promising to recover low-grade waste heat.[9]

TOEC can transform thermal energy to pressure difference efficiently. The question lies in whether one can obtain thermal energy efficiently by the reverse process. In this Letter we present a new type of hydraulic heat pump based on the RTO effect in a nanoporous membrane system, as shown in Figure 1b. The heat pump relies on a hydrophobic membrane and a vapor gap to separate two liquid regions. Similar to reverse osmosis, if a hydraulic pressure is used to overcome the thermo-osmotic effect, the working fluid evaporates from the cold side and condenses in the other side, bringing thermal energy to the hot side.[13−15]

RTO is a process controlled by kinetics and thermodynamic theory.[16] As shown in Figure 1c, to study the energy- and mass-transfer performances of RTO, we built and performed classical MD simulations to study the process. We predicted that the system performance mainly depends on its transport capabilities and the working pressure.[17−19] As shown in Figure 1d, to keep the system from pore wetting by a large working pressure, an NPG membrane was employed and its pores are hydrogenated to get hydrophobicity, with diameters of

Received: August 13, 2020
Accepted: September 29, 2020
Published: September 29, 2020

https://dx.doi.org/10.1021/acs.jpclett.0c02475
J. Phys. Chem. Lett. 2020, 11, 9856−9861

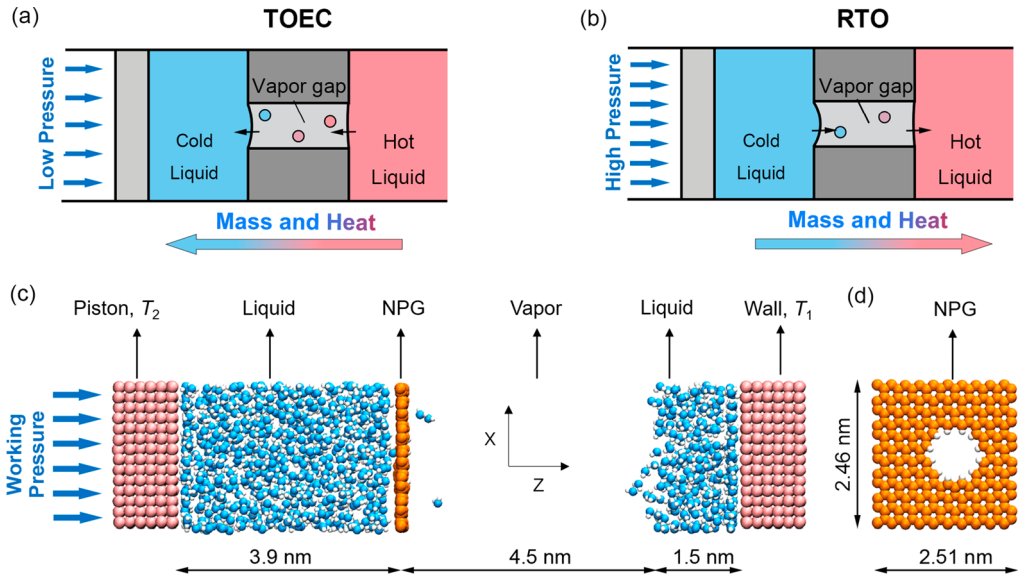

Figure 1. (a and b) Schematic illustrations of thermo-osmotic energy conversion (TOEC) and reverse thermo-osmosis (RTO) processes in vapor-gap membranes. The temperature differences across the membranes can generate thermo-osmotic pressures. For the TOEC process, the working pressure difference is lower than the thermo-osmotic pressure, and the working fluid moves from the hot side to the cold side by evaporation and condensation. For the RTO process, the working pressure difference is higher, and the working fluid will be transferred inversely. (c) Side view of the simulation domain. The working fluid is water; the membrane type is the nanoporous graphene (NPG), and the piston and the wall are made of copper. The two liquid layers are separated by an NPG membrane and a vapor layer. A working pressure can be added to the piston uniformly. (d) Top view of the NPG membrane. The pore is hydrogenated, and its diameter is about 0.8 nm.

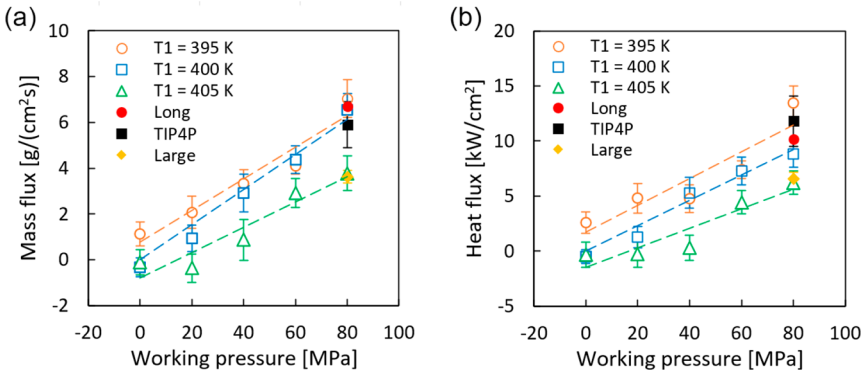

Figure 2. Fluxes of the RTO system: (a) mass fluxes and (b) heat fluxes. The temperature of the wall, T_1, varies with cases, and the temperature of the piston, T_2, remains 400 K. The fluxes are increased linearly with working pressures. The low wall temperature of 395 K promotes the fluxes while the high temperature of 405 K reduces the fluxes. The red circle and black square represent the results carrying out for a long time of 10 ns or employing the TIP4P water model with T_1 = 400 K, which are in good agreement with the main cases. The yellow rhombuses represent the results with a 1.52 times larger membrane size, a same pore size, and T_1 = 400 K, which have lower fluxes. All fluxes are the total fluxes of the membrane region. The intercepts of the trend lines for T_1 = 400 K are set to 0. The bars represent standard errors.

approximately 0.8 nm. NPG membranes have good mechanical properties with a thickness of approximately 0.35 nm for a single layer and have drawn wide attention for separation and energy conversion.[20−22] The preparation technologies of large-area NPG membranes are also developing quickly, which lay the foundations for commercial applications.[23,24]

The simulations were built and carried out by the LAMMPS package and visualized by the VMD.[25,26] The size of the simulation domain is 2.46 × 2.51 × 14.0 nm^3, and periodic boundaries were applied in the x and y directions. As vaporization and condensation are the transfer processes combining mass and heat, for the main simulation processes, the temperatures of heat sources were controlled by Langevin method, and the remaining parts were integrated with the *NVE* method to simulate the heat-transfer process.[27] A modified TIP3P water model was chosen to describe vapor and liquid properties exactly,[28] and the AIREBO potential was employed to simulate the heat conduction in the NPG membrane.[29] More details are in the Supporting Information (SI 1).

To get the basic properties of the system, we computed the mass- and heat-transfer process under hydraulic pressures. The hydraulic pressures were varied from 0 to 80 MPa, while a too high pressure might lead to an overflow. The piston temperatures were maintained at 400 K in all cases, and the temperatures of the copper wall in the other side were changed from 395, 400, and 405 K. Each case was carried out for 2 ns and repeated 12 times. Mass fluxes of the system were obtained by counting water molecule changes in the wall side, and heat fluxes were found from the enthalpy change of the wall. As shown in Figure 2, results show that the fluxes are increased

https://dx.doi.org/10.1021/acs.jpclett.0c02475
J. Phys. Chem. Lett. 2020, 11, 9856−9861

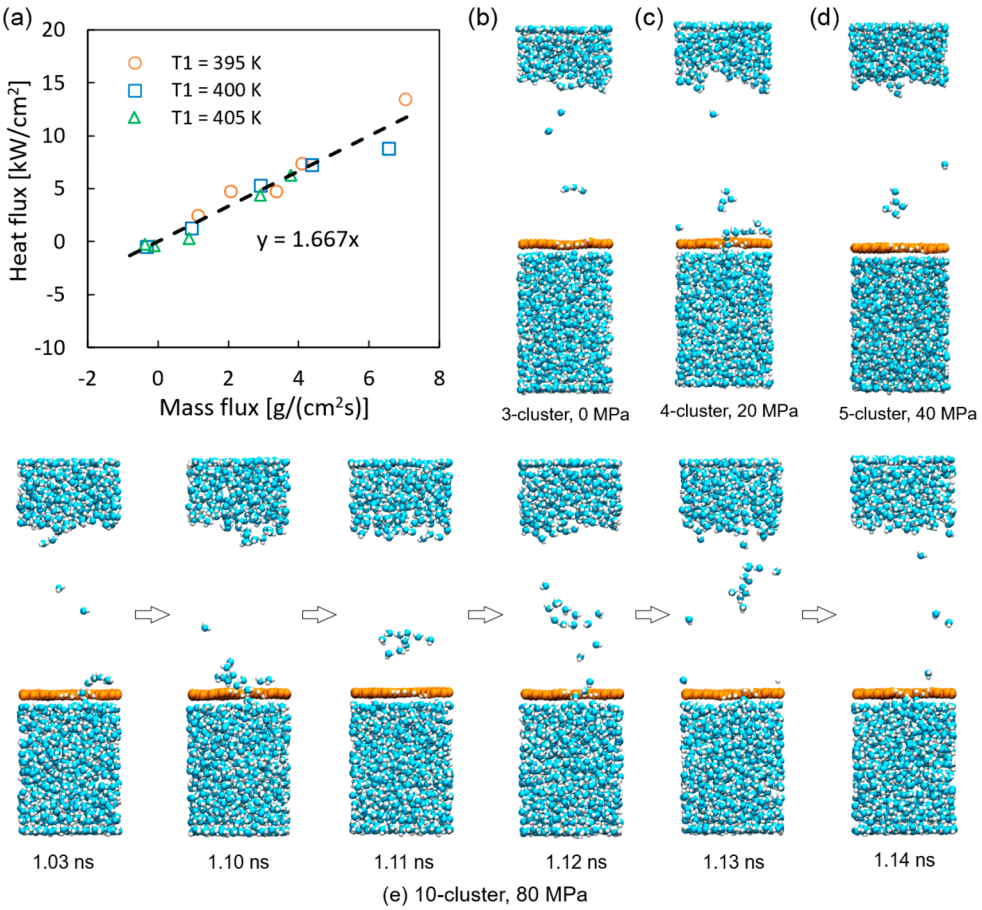

Figure 3. (a) Heat fluxes are in proportion to the mass fluxes with a ratio of 1.667 kJ/g, much lower than the standard vaporization enthalpy of water, 2.183 kJ/g at 400 K. (b–d) Views of cluster evaporations, of which copper atoms are hidden (e) Process views of a 10-cluster evaporation. Half of the membrane is hidden to make the processes more clear. Water molecules on the NPG membrane can evaporate as clusters, which should be the reason why the evaporation heats are reduced.

linearly with the work pressure, because the driving forces of mass transfer are the vapor pressure differences of the two sides, and from the Kelvin equation, the vapor pressure differences change linearly with the hydraulic pressures when the hydraulic pressures are not too high.[9] Because heat transfer relies on the mass transfers mainly by phase change, the heat fluxes are varied with the mass fluxes. As in our predictions (similar to SI 9), the fluxes are also influenced by the temperatures of the wall, and the low wall temperatures improve the fluxes while the higher temperatures reduce them. For the case with a working pressure of 80 MPa and T_1 = 405 K, it transfers heat from a low-temperature source to a higher source with a temperature increment of 5 K; heat fluxes of 6.2 ± 1.0 kW/cm^2; and a COP of approximately 20.2, which is defined as the ratio of heat transferred to the power supplied.

The COP of the system can be estimated by COP = $\rho_l h_t / p_w$, where ρ_l is the density of water; h_t is the ratio of the heat transferred to the mass transferred; p_w is the working pressure. To get the values of h_t, the relationship between heat fluxes and mass fluxes are shown in Figure 3a. The heat fluxes scale linearly with mass fluxes. But unexpectedly, the ratio is only 1.667 kJ/g, much less than the standard vaporization enthalpy of water at 400 K, 2.183 kJ/g for a physical value[30] or 2.160 kJ/g for the MD value (SI 2). The heat fluxes should include heat transfer by convection and phase change. However, the wall temperatures have little influence on the h_t, so the heat transfer by convection can be ignored relative to that by mass transfer, and the h_t measured should be the vaporization enthalpy of the processes. The decrease of vaporization enthalpy reduces the COP of the system. For the case with a working pressure of 80 MPa and T_1 = 405 K, the COP is reduced from 26.2 to 20.2. To investigate the mechanism of reduced vaporization enthalpy, we made several investigations and found that the reason should be that water molecules on the NPG membrane can evaporate incompletely in a cluster state, shown in Figure 3b–e.

The microstructure of water in liquid and ice are clusters connected by the hydrogen-bonding network, which plays an important role in the dynamics of water, and has received great attention.[31−33] The phenomenon of cluster evaporation was first reported by the studies of seawater distillation in hydrogels, which can reduce the heat demand of solar vapor generation.[34,35] In this work, we found that cluster evaporation can also happen on the NPG membrane. As shown in Figure 3b–e, water molecules can pass through NPG as clusters containing several molecules, which exhibits the distinctive nanoscale effect of nanoconfined fluids.[36,37] The detailed structures of the clusters are shown in SI 4. According to our observation, cluster evaporation can happen at all pressure conditions from 0 to 80 MPa, and a large water cluster is generated more easily in the case with a high working pressure. As shown in Figure 3e, a typical cluster evaporation consists of 3 steps: (1) water molecules pass through the pore from the liquid region to the upper surface of the NPG membrane; (2)

https://dx.doi.org/10.1021/acs.jpclett.0c02475
J. Phys. Chem. Lett. 2020, 11, 9856−9861

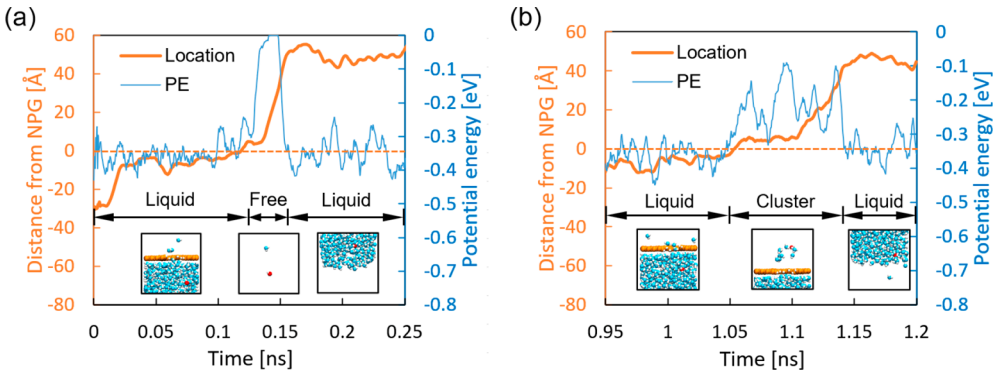

Figure 4. Location evaluations in the *z*-direction and the potential energy (PE) evaluations of water molecules during the transfer processes: (a) a water molecule vaporized completely; (b) a water molecule evaporated within a 10-cluster. The two molecules are marked red, and they are selected from the case with a pressure of 80 MPa (the same as Figure 3e). The results show that a cluster water molecule has a PE of about −0.24 eV, lower than that of a free vapor molecule about 0 eV, meaning that cluster evaporations absorb less heat than complete evaporations.

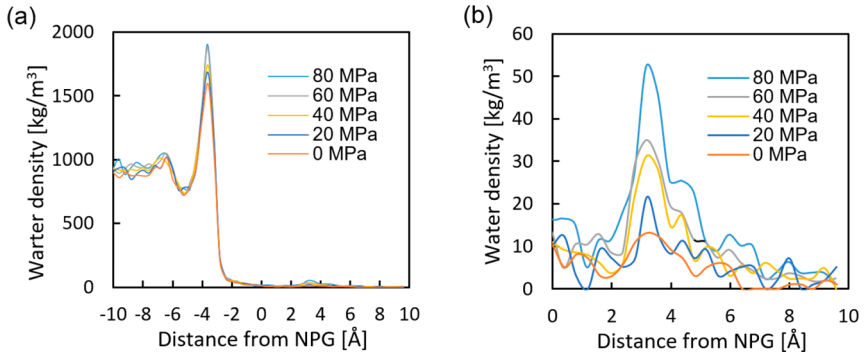

Figure 5. Water densities with relative distances to NPG membrane at different hydraulic pressures: (a) density distribution near the NPG membrane and (b) local zoom on the NPG membrane surface. The high-pressure cases have higher water densities in bulk liquid compared to the lower. Water molecules have more probability to move across the NPG membrane and form clusters with help of a high hydraulic pressure.

water molecules form a cluster and stay on the NPG membrane for several picoseconds; (3) the cluster can depart from the membrane and enter to the vapor region with a probability, while clusters are more likely to recede into the bulk liquid (SI 5).

To probe the physical mechanism of the cluster evaporation, we computed the location and potential energy (PE) evolutions of water molecules. Figure 4a shows the results of a water molecule evaporate completely, and Figure 4b presents cluster evaporation. For both cases, the locations of the molecules change gradually from the NPG side to the wall side, and the molecules have experienced stages of liquid, free/cluster, and liquid. The PEs are varied with the molecule states, from low to high when molecules change to free/cluster state, and back to low when they condense. It is noted that the PE of a cluster molecule is much lower than that of a free molecule, meaning that cluster evaporations absorb less heat than complete evaporations for the same mass. The results prove that cluster evaporations on the NPG membrane reduce the vaporization enthalpy of the RTO system.

In addition, Figure 4b shows the PE of a cluster molecule is higher than that of a liquid molecule, which indicates that it is an unstable state for a cluster staying on the NPG membrane (1.05−1.1 ns), and clusters have a tendency to recede to the bulk liquid region (SI 3). The water density distributions in the *z*-direction are shown in Figure 5. Figure 5a shows that there are small density peaks near 4 Å, induced by the clusters staying on the NPG membrane. Figure 5b clearly shows that the water densities on NPG are promoted significantly by the working pressures, indicating water molecules have more probability to move across NPG membrane and form clusters under a higher pressure. Because the formation of a cluster needs to overcome a PE difference, it is reasonable that a high working pressure can help the process.[38]

In summary, we have studied RTO processes in the NPG membrane regime by classical MD simulations. The RTO system can transfer heat and mass efficiently by driving forces of hydraulic pressure. Superhigh heat fluxes of 6.2 ± 1.0 kW/cm^2 and COP of 20.2 are achieved with a temperature increment of 5 K. The results show that RTO processes have wide potential implication for heat pumps, and other transfer processes including water desalination, vapor generation, and heat dissipation. The heat and mass fluxes of the RTO system vary linearly with work pressure, and the fluxes are also influenced by the temperature difference. The heat transfer relies on phase changes and the mass transfer, and the heat fluxes are in proportion to the mass fluxes. Water cluster evaporation can happen on an NPG membrane and reduces the vaporization enthalpy of the processes.

■ ASSOCIATED CONTENT

Supporting Information

The Supporting Information is available free of charge at https://pubs.acs.org/doi/10.1021/acs.jpclett.0c02475.

Simulation details; details of COP calculation; vaporization heat measure; cluster structures; views of a

https://dx.doi.org/10.1021/acs.jpclett.0c02475
J. Phys. Chem. Lett. 2020, 11, 9856−9861

cluster receding; sustainability check; size effect check; model sensibility check; theoretical analysis of a large-scale RTO system (PDF)

AUTHOR INFORMATION

Corresponding Author

Zhichun Liu − *School of Energy and Power Engineering, Huazhong University of Science and Technology, Wuhan 430074, China;* orcid.org/0000-0001-9645-3052; Email: zcliu@hust.edu.cn

Authors

Ji Li − *School of Energy and Power Engineering, Huazhong University of Science and Technology, Wuhan 430074, China*

Rui Long − *School of Energy and Power Engineering, Huazhong University of Science and Technology, Wuhan 430074, China;* orcid.org/0000-0003-4911-1716

Bo Zhang − *School of Energy and Power Engineering, Huazhong University of Science and Technology, Wuhan 430074, China*

Ronggui Yang − *School of Energy and Power Engineering, Huazhong University of Science and Technology, Wuhan 430074, China;* orcid.org/0000-0002-3602-6945

Wei Liu − *School of Energy and Power Engineering, Huazhong University of Science and Technology, Wuhan 430074, China*

Complete contact information is available at: https://pubs.acs.org/10.1021/acs.jpclett.0c02475

Notes

The authors declare no competing financial interest.

ACKNOWLEDGMENTS

The authors thank the National Supercomputer Center in Tianjin for providing computing resources. The study was supported by the National Natural Science Foundation of China (No. 52076088 and No. 51776079) and the Open Research Fund of Key Laboratory of Space Utilization, Chinese Academy of Sciences (No. LSU-KFJJ-2019-07).

REFERENCES

(1) *Fuels and technologies*. International Energy Agency. https://www.iea.org/fuels-and-technologies.

(2) Song, M.; Deng, S.; Dang, C.; Mao, N.; Wang, Z. Review on Improvement for Air Source Heat Pump Units during Frosting and Defrosting. *Appl. Energy* **2018**, *211*, 1150−1170.

(3) Li, W.; Xia, X.; Cao, M.; Li, S. Structure-Property Relationship of Metal-Organic Frameworks for Alcohol-Based Adsorption-Driven Heat Pumps via High-Throughput Computational Screening. *J. Mater. Chem. A* **2019**, *7*, 7470−7479.

(4) Kishore, R. A.; Nozariasbmarz, A.; Poudel, B.; Sanghadasa, M.; Priya, S. Ultra-High Performance Wearable Thermoelectric Coolers with Less Materials. *Nat. Commun.* **2019**, *10*, 1765.

(5) Sweetnam, T.; Fell, M.; Oikonomou, E.; Oreszczyn, T. Domestic Demand-Side Response with Heat Pumps: Controls and Tariffs. *Build. Res. Inf.* **2019**, *47* (4), 344−361.

(6) Li, T.; Zhai, Y.; He, S.; Gan, W.; Wei, Z.; Heidarinejad, M.; Dalgo, D.; Mi, R.; Zhao, X.; Song, J.; et al. A Radiative Cooling Structural Material. *Science* **2019**, *364* (6642), 760−763.

(7) Barragán, V. M.; Kjelstrup, S. Thermo-osmosis in membrane systems: a review. *J. Non-Equilib. Thermodyn.* **2017**, *42* (3), 217−236.

(8) Marbach, S.; Bocquet, L. Osmosis, from Molecular Insights to Large-Scale Applications. *Chem. Soc. Rev.* **2019**, *48*, 3102−3144.

(9) Straub, A. P.; Elimelech, M. Energy Efficiency and Performance Limiting Effects in Thermo-Osmotic Energy Conversion from Low-Grade Heat. *Environ. Sci. Technol.* **2017**, *51* (21), 12925−12937.

(10) Straub, A. P.; Yip, N. Y.; Lin, S.; Lee, J.; Elimelech, M. Harvesting Low-Grade Heat Energy Using Thermo-Osmotic Vapour Transport through Nanoporous Membranes. *Nat. Energy* **2016**, *1*, 16090.

(11) Yuan, Z.; Wei, L.; Afroze, J. D.; Goh, K.; Chen, Y.; Yu, Y.; She, Q.; Chen, Y. Pressure-Retarded Membrane Distillation for Low-Grade Heat Recovery: The Critical Roles of Pressure-Induced Membrane Deformation. *J. Membr. Sci.* **2019**, *579*, 90−101.

(12) Chen, X.; Boo, C.; Yip, N. Y. Low-Temperature Heat Utilization with Vapor Pressure-Driven Osmosis: Impact of Membrane Properties on Mass and Heat Transfer. *J. Membr. Sci.* **2019**, *588*, 117181.

(13) Li, W.; Yang, Y.; Weber, J. K.; Zhang, G.; Zhou, R. Tunable, Strain-Controlled Nanoporous MoS2 Filter for Water Desalination. *ACS Nano* **2016**, *10* (2), 1829−1835.

(14) Lee, J.; Karnik, R. Desalination of Water by Vapor-Phase Transport through Hydrophobic Nanopores. *J. Appl. Phys.* **2010**, *108*, 044315.

(15) Nomura, K.; Nishihara, H.; Yamamoto, M.; Gabe, A.; Ito, M.; Uchimura, M.; Nishina, Y.; Tanaka, H.; Miyahara, M. T.; Kyotani, T. Force-Driven Reversible Liquid−Gas Phase Transition Mediated by Elastic Nanosponges. *Nat. Commun.* **2019**, *10*, 2559.

(16) Fu, L.; Merabia, S.; Joly, L. Understanding Fast and Robust Thermo-Osmotic Flows through Carbon Nanotube Membranes: Thermodynamics Meets Hydrodynamics. *J. Phys. Chem. Lett.* **2018**, *9*, 2086−2092.

(17) Li, J.; Gao, S.; Long, R.; Liu, W.; Liu, Z. Self-Pumped Evaporation for Ultra-Fast Water Desalination and Power Generation. *Nano Energy* **2019**, *65*, 104059.

(18) Lu, Z.; Wilke, K. L.; Preston, D. J.; Kinefuchi, I.; Chang-Davidson, E.; Wang, E. N. An Ultrathin Nanoporous Membrane Evaporator. *Nano Lett.* **2017**, *17* (10), 6217−6220.

(19) Lu, Z.; Kinefuchi, I.; Wilke, K. L.; Vaartstra, G.; Wang, E. N. A Unified Relationship for Evaporation Kinetics at Low Mach Numbers. *Nat. Commun.* **2019**, *10*, 2368.

(20) Garnier, L.; Szymczyk, A.; Malfreyt, P.; Ghoufi, A. Physics behind Water Transport through Nanoporous Boron Nitride and Graphene. *J. Phys. Chem. Lett.* **2016**, *7* (17), 3371−3376.

(21) Kang, Y.; Xia, Y.; Wang, H.; Zhang, X. 2D Laminar Membranes for Selective Water and Ion Transport. *Adv. Funct. Mater.* **2019**, *29* (29), 1902014.

(22) Macha, M.; Marion, S.; Nandigana, V. V. R.; Radenovic, A. 2D Materials as an Emerging Platform for Nanopore-Based Power Generation. *Nat. Rev. Mater.* **2019**, *4*, 588−605.

(23) Yang, Y.; Yang, X.; Liang, L.; Gao, Y.; Cheng, H.; Li, X.; Zou, M.; Cao, A.; Ma, R.; Yuan, Q.; et al. Large-Area Graphene-Nanomesh/ Carbon-Nanotube Hybrid Membranes for Ionic and Molecular Nanofiltration. *Science* **2019**, *364* (6445), 1057−1062.

(24) Zhang, Y.; De Aguiar, H. B.; Hynes, J. T.; Laage, D. Water Structure, Dynamics, and Sum-Frequency Generation Spectra at Electrified Graphene Interfaces. *J. Phys. Chem. Lett.* **2020**, *11*, 624.

(25) Plimpton, S. Fast Parallel Algorithms for Short-Range Molecular Dynamics. *J. Comput. Phys.* **1995**, *117*, 1−42.

(26) Humphrey, W.; Dalke, A.; Schulten, K. VMD: Visual Molecular Dynamics. *J. Mol. Graphics* **1996**, *14*, 33−38.

(27) Liu, R.; Liu, Z. Study of Boiling Heat Transfer on Concave Hemispherical Nanostructure Surface with MD Simulation. *Int. J. Heat Mass Transfer* **2019**, *143*, 118534.

(28) Price, D. J.; Brooks, C. L. A Modified TIP3P Water Potential for Simulation with Ewald Summation. *J. Chem. Phys.* **2004**, *121*, 10096.

(29) O'Connor, T. C.; Andzelm, J.; Robbins, M. O. AIREBO-M: A Reactive Model for Hydrocarbons at Extreme Pressures. *J. Chem. Phys.* **2015**, *142*, 024903.

(30) Thermophysical Properties of Fluid Systems. *Chemistry Web Book, SDR 69*; National Institution of Standards and Technology (NIST). https://webbook.nist.gov/chemistry/fluid/.
(31) Malloum, A.; Fifen, J. J.; Dhaouadi, Z.; Nana Engo, S. G.; Conradie, J. Structures, Relative Stability and Binding Energies of Neutral Water Clusters, (H2O)2−30. *New J. Chem.* **2019**, *43*, 13020−13037.
(32) Yoo, S.; Aprà, E.; Zeng, X. C.; Xantheas, S. S. High-Level Ab Initio Electronic Structure Calculations of Water Clusters (H2O)16 and (H2O)17: A New Global Minimum for (H2O)16. *J. Phys. Chem. Lett.* **2010**, *1* (20), 3122−3127.
(33) Shiotari, A.; Sugimoto, Y. Ultrahigh-Resolution Imaging of Water Networks by Atomic Force Microscopy. *Nat. Commun.* **2017**, *8*, 14313.
(34) Zhao, F.; Zhou, X.; Shi, Y.; Qian, X.; Alexander, M.; Zhao, X.; Mendez, S.; Yang, R.; Qu, L.; Yu, G. Highly Efficient Solar Vapour Generation via Hierarchically Nanostructured Gels. *Nat. Nanotechnol.* **2018**, *13*, 489−495.
(35) Zhou, X.; Zhao, F.; Guo, Y.; Rosenberger, B.; Yu, G. Architecting Highly Hydratable Polymer Networks to Tune the Water State for Solar Water Purification. *Sci. Adv.* **2019**, *5* (6), No. eaaw5484.
(36) Sun, C.; Zhou, R.; Zhao, Z.; Bai, B. Nanoconfined Fluids: What Can We Expect from Them? *J. Phys. Chem. Lett.* **2020**, *11* (12), 4678−4692.
(37) Zhong, J.; Alibakhshi, M. A.; Xie, Q.; Riordon, J.; Xu, Y.; Duan, C.; Sinton, D. Exploring Anomalous Fluid Behavior at the Nanoscale: Direct Visualization and Quantification via Nanofluidic Devices. *Acc. Chem. Res.* **2020**, *53* (2), 347−357.
(38) Xu, F.; Wei, M.; Zhang, X.; Song, Y.; Zhou, W.; Wang, Y. How Pore Hydrophilicity Influences Water Permeability? *Research* **2019**, *2019*, 2581241.

https://dx.doi.org/10.1021/acs.jpclett.0c02475
J. Phys. Chem. Lett. 2020, 11, 9856−9861